Pergamon

0045-7949(94)00427-7

Computers & Structures Vol. 55, No. 5, pp. 857–870, 1995
Elsevier Science Ltd
Printed in Great Britain
0045-7949/95 $9.50 + 0.00

PARAMETRIC INSTABILITY OF A SANDWICH BEAM UNDER VARIOUS BOUNDARY CONDITIONS

K. Ray and **R. C. Kar**

Department of Mechanical Engineering, Indian Institute of Technology, Kharagpur 721302, India

(*Received* 19 *September* 1993)

Abstract—Parametric instability of a three-layered symmetric sandwich beam subjected to a periodic axial load is considered under nine different boundary conditions. The influence of static load parameter and core-thickness parameter on the system loss factor is investigated. The effect of shear parameter on the static buckling loads is also considered, besides, the effects of shear parameter, core thickness parameter and core loss factor on the regions of parametric instability are studied.

1. INTRODUCTION

It is well-known that a layer of viscoelastic material sandwiched between two elastic metallic layers has remarkable vibration damping capabilities; this has resulted in rapid development of sandwich structures for use in aircraft and other industries. Kerwin [1] was the first to develop a theory for the damping of flexural waves by a viscoelastic damping layer. DiTaranto [2] derived the sixth order, complex, homogeneous differential equation for finite length sandwich beams. Mead and Markus [3] studied the forced vibration of a three-layered damped sandwich beam with arbitrary boundary conditions. Asnani and Nakra [4, 5] considered vibration damping characteristics of multilayered sandwich beams. Rao [6] obtained loss factors of a pre-twisted, simply-supported sandwich beam. Rao and Stühler [7] considered a tapered sandwich beam and investigated its damping effectiveness for simply-supported and clamped–free configurations. Rao [8] obtained accurate loss and frequency factors of a simply-supported short sandwich beam by considering higher order effects. He later [9] obtained the frequency and loss factors of sandwich beams under several boundary conditions. He also studied [10] the forced vibration of a damped sandwich beam subjected to moving forces. Ko [11] studied the flexural behaviour of a rotating, tapered sandwich beam.

Little work seems to be reported on the stability of sandwich beams. Bauld [12] considered the dynamic stability of sandwich columns with pinned ends under pulsating axial loads. Chonan studied the stability of two-layered [13] and three-layered [14] cantilevered sandwich beams with imperfect, elastic bonding subjected to constant horizontal and tangential compressive forces. In a more recent work [15], Kar and Sujata studied the dynamic stability of a tapered, symmetric sandwich beam.

The purpose of the present work is to study the parametric instability of a three-layered, symmetric sandwich beam subjected to a periodic axial load under nine different boundary conditions. Equations of motion are derived by Hamilton's principle. A generalized Galerkin's method is used to reduce the non-dimensional equations of motion to a set of coupled Hill's equations with complex coefficients. The regions of instability for simple and combination resonances are obtained by modified Hsu's [16] method, using conditions given in [17]. The influences of static load parameter and core thickness parameter on the fundamental system loss factor, the effect of shear parameter on the fundamental static buckling load and the effects of shear parameter, core thickness parameter and core loss factor on the instability regions are investigated.

2. FORMULATION OF THE PROBLEM

Figure 1 shows a three-layered symmetric sandwich beam of length L. A periodic force $P(t) = P_0 + P_1 \cos \omega t$ acts axially on it as shown, ω being the frequency of the applied load, t being the time and P_0 and P_1 being, respectively, the static and dynamic load amplitudes. The beam may be subjected to any of the boundary conditions listed in Table 1. The face layers of the beam are of the same material, each having thickness $2h_1$ and Young's modulus E_1. The core is viscoelastic with a complex shear modulus $G_2^* = G_2(1 + \mathrm{j}\eta_c)$, G_2 being the in-phase shear modulus, η_c the core loss factor and $\mathrm{j} = \sqrt{-1}$.

With the assumptions of Rao [9], and using Hamilton's principle, the non-dimensional equations of motion for coupled transverse and axial vibrations are

$$\bar{w}_{,\bar{t}\bar{t}} + (1 + Y)\bar{w}_{,\bar{x}\bar{x}\bar{x}\bar{x}} + \bar{P}\bar{w}_{,\bar{x}\bar{x}} - Y\bar{u}_{,\bar{x}\bar{x}\bar{x}} = 0, \quad (1)$$

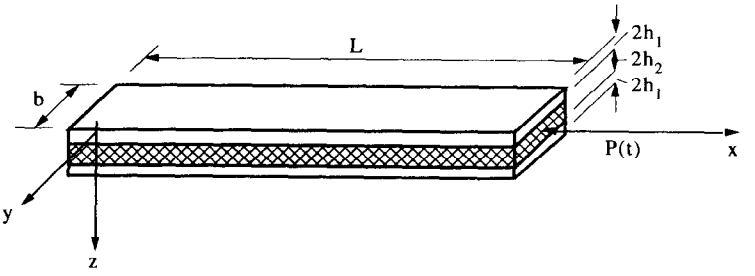

Fig. 1. Configuration of the system.

$$\bar{w}_{,\bar{x}\bar{x}\bar{x}} - \ddot{\bar{u}}_{,\bar{x}\bar{x}} + g^* h_{12}^2 \ddot{\bar{u}} = 0, \quad 0 < \bar{x} < 1, \quad \bar{t} \geqslant 0, \quad (2)$$

subject to the boundary conditions:

$$\left.\begin{array}{lll} \bar{M} = 0 & \text{or,} & \bar{w}_{,\bar{x}} = 0, \\ \bar{Q} = -\bar{P}\bar{w}_{,\bar{x}} & \text{or} & \bar{w} = 0 \\ \text{and} \quad \bar{N} = 0 & \text{or,} & \bar{u} = 0 \end{array}\right| \quad (3)$$

at either end of the beam, where

$$\bar{M} = (1 + Y)\bar{w}_{,\bar{x}\bar{x}} - Y\bar{u}_{,\bar{x}},$$

$$\bar{Q} = (1 + Y)\bar{w}_{,\bar{x}\bar{x}\bar{x}} - Y\bar{u}_{,\bar{x}\bar{x}},$$

and

$$\bar{N} = \bar{w}_{,\bar{x}\bar{x}} - \bar{u}_{,\bar{x}}.$$

In eqns (1)–(3),

$$\bar{w}(\bar{x}, \bar{t}) = w(x, t)/L, \quad \bar{u}(\bar{x}, \bar{t}) = u(x, t)/L,$$

w being the beam transverse displacement and u being related to the shear strain γ_2 in the core layer through the relationship $u = \{L/(1 + h_{12})\}\ \gamma_2$, where $h_{12} = h_1/h_2 = 1/h_{21}$, $\bar{x} = x/L$, the non-dimensional time $\bar{t} = t/t_0$, $t_0 = [mL^4/(2E_1 I_1)]^{1/2}$, m = mass/unit length of the beam, $2E_1 I_1$ = beam flexural rigidity, neglecting the flexural rigidity of the core,

$$Y = 3(1 + h_{21})^2, \quad \bar{P} = \bar{P}_0 + \bar{P}_1 \cos \bar{\omega}\bar{t},$$

$$\bar{P} = PL^2/(2E_1 I_1),$$

$$\bar{P}_0 = P_0 L^2/(2E_1 I_1),$$

$$\bar{P}_1 = P_1 L^2/(2E_1 I_1), \quad \bar{\omega} = \omega t_0,$$

$$g^* = (G_2^*/2E_1)(h_{21})(L/h_1)^2 = g(1 + \mathrm{j}\eta_c),$$

where $g = (G_2/2E_1)(h_{21})(L/h_1)^2$ is the shear parameter,

$$\bar{w}_{,\bar{x}} = \partial\bar{w}/\partial\bar{x}, \quad \dot{\bar{w}}_{,\bar{t}} = \partial\dot{\bar{w}}/\partial\bar{t}, \text{ etc.}$$

The various end arrangements considered and the associated boundary conditions are given in Table 1.

3. APPROXIMATE SOLUTION

Solutions of (1) and (2) are assumed in the form

$$\bar{w}(\bar{x}, \bar{t}) = \sum_{i=1}^{r} q_i(\bar{t}) w_i(\bar{x}), \quad (4a)$$

$$\bar{u}(\bar{x}, \bar{t}) = \sum_{k=r+1}^{s} q_k(\bar{t}) u_k(\bar{x}), \quad (4b)$$

where $q_{v_1}(\bar{t})$, $v_1 = 1, 2, \ldots, s$, denote the generalized coordinates and $w_i(\bar{x})$, $u_k(\bar{x})$ are the coordinate functions chosen to satisfy as many of the boundary conditions (3) as possible. It is further assumed that the coordinate functions for the various boundary

Table 1. End arrangements and boundary conditions

Boundary arrangement			Boundary conditions to be satisfied	
No.	Description	Abbreviation	Left end of beam ($\bar{x} = 0$)	Right end of beam ($\bar{x} = 1$)
1.	Pinned–Pinned	P–P	$\bar{w} = \bar{M} = \bar{N} = 0$	$\bar{w} = \bar{M} = \bar{N} = 0$
2.	Pinned–Pinned riveted	P–PR	$\bar{w} = \bar{M} = \bar{N} = 0$	$\bar{w} = \bar{M} = \bar{u} = 0$
3.	Guided–Pinned	G–P	$\bar{w}_{,\bar{x}} = \bar{Q} = \bar{N} = 0$	$\bar{w} = \bar{M} = \bar{N} = 0$
4.	Clamped–Free	C–F	$\bar{w} = \bar{w}_{,\bar{x}} = \bar{u} = 0$	$\bar{Q} = \bar{M} = \bar{N} = 0$
5.	Clamped–Pinned	C–P	$\bar{w} = \bar{w}_{,\bar{x}} = \bar{u} = 0$	$\bar{w} = \bar{M} = \bar{N} = 0$
6.	Clamped–Guided	C–G	$\bar{w} = \bar{w}_{,\bar{x}} = \bar{u} = 0$	$\bar{w}_{,\bar{x}} = \bar{Q} = \bar{N} = 0$
7.	Clamped–Clamped	C–C	$\bar{w} = \bar{w}_{,\bar{x}} = \bar{u} = 0$	$\bar{w} = \bar{w}_{,\bar{x}} = \bar{u} = 0$
8.	Clamped–Free riveted	C–FR	$\bar{w} = \bar{w}_{,\bar{x}} = \bar{u} = 0$	$\bar{Q} = \bar{M} = \bar{u} = 0$
9.	Clamped–Clamped unrestrained	C–CUR	$\bar{w} = \bar{w}_{,\bar{x}} = \bar{u} = 0$	$\bar{w} = \bar{w}_{,\bar{x}} = \bar{N} = 0$

Table 2. The co-ordinate functions, $\mu_1 = Y/(1+Y)$, $\mu_2 = \bar{P}_0/(1+Y)$

End arrangement	Coordinate function ($i = 1, 2, \ldots, r$, $k = \{(r+1), \ldots, s\}$, $\bar{k} = k - r$)
P–P	$w_i(\bar{x}) = \sin(\pi i \bar{x}), \quad u_k(\bar{x}) = \cos(\pi \bar{k} \bar{x})$
P–PR	$w_i(\bar{x}) = \bar{x} - (-1)^{(i+1)} \sin\{(2i-1)\pi\bar{x}/2\}$, $u_k(\bar{x}) = (-1)^{\bar{k}}\{(2\bar{k}-1)\pi/2\mu_1\}\cos\{(2\bar{k}-1)\pi\bar{x}/2\}$.
G–P	$w_i(\bar{x}) = \cos\{(2i-1)\pi\bar{x}/2\}$, $u_k(\bar{x}) = -\{(2\bar{k}-1)\pi/2\}\sin\{(2\bar{k}-1)\pi\bar{x}/2\}$.
C–F	$w_i(\bar{x}) = (i+3)(i+2)\{(i+2)(i+1) - \mu_2\}\bar{x}^{(i+1)} + [2(i+3)(i+1)\{\mu_2 - i(i+2)\}$ $+ \mu_1 i(i+1)/\{(i+2)(i+1) - \mu_2\}]\bar{x}^{(i+2)}$ $+ [(i+2)(i+1)\{-\mu_2 + i(i+1)\} - \mu_1 i(i+1)^2$ $/\{(i+3)(i+2)(i+1) - (i+3)\mu_2\}]\bar{x}^{(i+3)}$, $u_k(\bar{x}) = (\bar{k}+1)\bar{x}^{\bar{k}} - \bar{k}\bar{x}^{(\bar{k}+1)}$
C–P	$w_i(\bar{x}) = 2(i+2)\bar{x}^{(i+1)} - (4i+6)\bar{x}^{(i+2)} + 2(i+1)\bar{x}^{(i+3)}$, $u_k(\bar{x}) = (\bar{k}+1)\bar{x}^{\bar{k}} - \bar{k}\bar{x}^{(\bar{k}+1)}$
C–G	$w_i(\bar{x}) = (i+3)(i+2)(i+1)\{2 + (2-\mu_1)i\}\bar{x}^{(i+1)} - [2(i+3)(i+1)^2\{1 + (2-\mu_1)i\}$ $+ \mu_1 i(i+1)/\{2(i+2) + (2-\mu_1)(i+2)i\}]\bar{x}^{(i+2)}$ $+ [(i+2)(i+1)^2 i(2-\mu_1) - \mu_1 i(i+1)/\{2(i+3) + (2-\mu_1)(i+3)i\}]\bar{x}^{(i+3)}$, $u_k(\bar{x}) = (\bar{k}+1)\bar{x}^{\bar{k}} - [2(\bar{k}+3)(\bar{k}+2)(\bar{k}+1) + \bar{k}\{1 + \mu_1/(2 + 2\bar{k} - \mu_1\bar{k})\}]\bar{x}^{(\bar{k}+1)}$
C–C	$w_i(\bar{x}) = \bar{x}^{(i+1)} - 2\bar{x}^{(i+2)} + \bar{x}^{(i+3)}$ $u_k(\bar{x}) = \bar{x}^{\bar{k}} - \bar{x}^{(\bar{k}+1)}$
C–FR	$w_i(\bar{x}) = (i+3)(i+2)\{(i+2)(i+1) - \mu_2\}\bar{x}^{(i+1)} + [2(i+3)(i+1)\{\mu_2 - i(i+2)\}$ $+ \mu_1\{(i-1)(i+2) - \mu_2\}/\{(i+2)^2(i+1) - \mu_2(i+2)\}]\bar{x}^{(i+2)}$ $+ [(i+2)(i+1)\{-\mu_2 + i(i+1)\} - \mu_1\{i(i+1) - \mu_2\}$ $/\{(i+3)(i+2)(i+1) - (i+3)\mu_2\}]\bar{x}^{(i+3)}$, $u_k(\bar{x}) = (\bar{k}+1)[\bar{x}^{\bar{k}} - \bar{x}^{(\bar{k}+1)}]$
C–CUR	$w_i(\bar{x}) = (i+3)(i+2)^2(i+1)\{\bar{x}^{(i+1)} - 2\bar{x}^{(i+2)} + \bar{x}^{(i+3)}\}$, $u_k(\bar{x}) = (\bar{k}+1)\bar{x}^{\bar{k}} + [2/(\bar{k}+1) - \bar{k}]\bar{x}^{(\bar{k}+1)}$

conditions can be approximated by the ones given in Table 2. These coordinate functions satisfy the associated simplified boundary conditions obtained from Table 1 by setting $\bar{P}_1 = 0$.

Substitution of eqn (4) in eqns (1) and (2) and use of the generalized Galerkin's method yield the following matrix eqns of motion in the generalized coordinates:

$$[M]\{\ddot{Q}_1\} + [K_{11}]\{Q_1\} + [K_{12}]\{Q_2\} = \{\phi\}, \quad (5)$$

$$[K_{21}]\{Q_1\} + [K_{22}]\{Q_2\} = \{\phi\}, \quad (6)$$

where

$$[K_{21}] = [K_{12}]^T, \quad \{Q_1\} = \{q_1, \ldots, q_r\}^T,$$

$$\{Q_2\} = \{q_{r+1}, \ldots, q_s\}^T, \quad (\dot{}) = \mathrm{d}(\,)/\mathrm{d}\bar{t}, \text{ etc.}$$

Elimination of $\{Q_2\}$ from eqns (5) and (6) leads to a more convenient form of the equation of motion:

$$[M]\{\ddot{Q}_1\} + [K]\{Q_1\} - \bar{P}_1 \cos\bar{\omega}\bar{t}\,[H]\{Q_1\} = \{\phi\}, \quad (7)$$

where

$$[K] = [\bar{K}_{11}] + \bar{P}_0[H] - [K_{12}][K_{22}]^{-1}[K_{12}]^T.$$

The elements of the various matrices are given as follows:

$$M_{ij} = \int_0^1 w_i w_j \,\mathrm{d}\bar{x}, \quad \bar{K}_{11_{ij}} = \int_0^1 (1+Y) w_{i,\bar{x}\bar{x}} w_{j,\bar{x}\bar{x}} \,\mathrm{d}\bar{x},$$

$$H_{ij} = -\int_0^1 w_{i,\bar{x}} w_{j,\bar{x}} \,\mathrm{d}\bar{x}, \quad K_{12_{ik}} = -\int_0^1 Y W_{i,\bar{x}\bar{x}} u_{k,\bar{x}} \,\mathrm{d}\bar{x},$$

$$K_{22_{kl}} = \int_0^1 [Y u_{k,\bar{x}} u_{l,\bar{x}} + g^* h_{12}^2 Y u_k u_l]\mathrm{d}\bar{x},$$

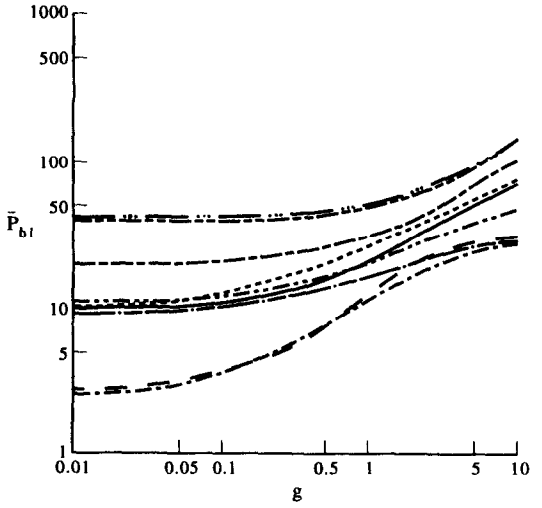

Fig. 2. Effect of shear parameter on the fundamental static buckling load with $\eta_c = 0.6$, $h_2/h_1 = 1$. —— P–P; - - - - P–PR; —— G–P; —·— C–F; —— — C–P; —·—·— C–G; —— — — C–C; —·— — C–FR; —·—·—C–CUR.

$$i, j = 1, 2, \ldots, r; \quad k, l = (r+1), \ldots, s.$$

In the above, $\{\phi\}$ denotes a null matrix.

If $[R]$ is the modal matrix corresponding to

$$[M]\{\ddot{Q}_1\} + [K]\{Q_1\} = \{\phi\}, \tag{8}$$

then use of the linear transformation

$$\{Q_1\} = [R]\{U\}, \tag{9}$$

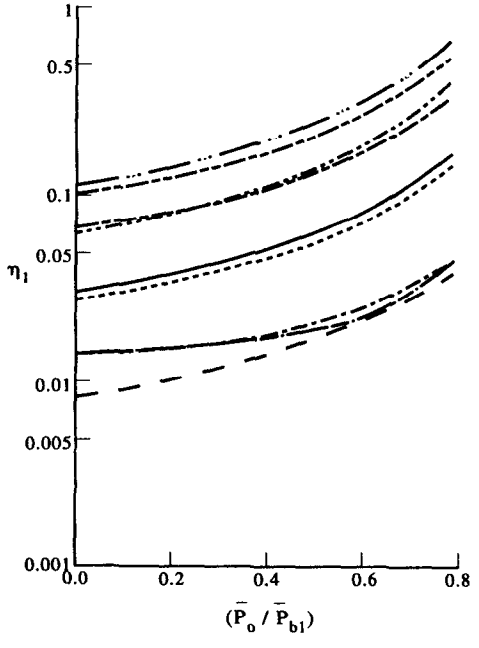

Fig. 3. Effect of static load parameter on the fundamental system loss factor with $\eta_c = 0.6$, $h_2/h_1 = 0.1$, $g = 1$. —— P–P; - - - - P–PR; —— G–P; —·— C–F; —— — C–P; —·—·— C–G; —— — — C–C; —·— — C–FR; —·—·— C–CUR.

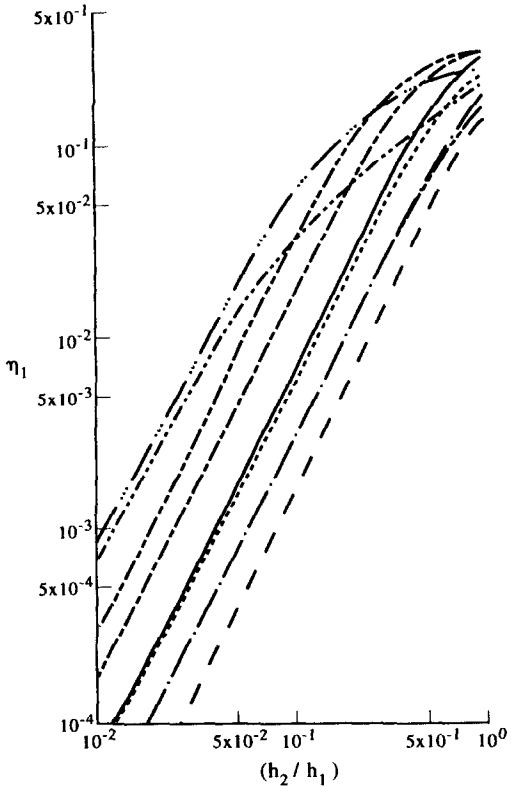

Fig. 4. Effect of core-thickness parameter on the fundamental system loss factor with $\eta_c = 0.6$, $g = 5.0$. —— P–P; - - - - P–PR; —— G–P; —·— C–F; —— — C–P; —·—·— C–G; —— — — C–C; —·— — C–FR; —·—·— C–CUR.

in which $\{U\}$ is a new set of generalized coordinates, transforms eqn (7) to the following set of equations:

$$\ddot{U}_N + \omega_N^{*2} U_N + 2\epsilon \cos \bar{\omega} \bar{t} \sum_{M=1}^{s} b_{NM}^{*} U_M = 0,$$

$$N = 1, 2, \ldots, r. \tag{10}$$

ω_N^{*2} are the distinct complex eigenvalues of $[M]^{-1}[K]$ and b_{NM}^{*} are the elements of the complex matrix

$$[B] = -[R]^{-1}[M]^{-1}[H][R], \quad \epsilon = \bar{P}_1/2 < 1.$$

For subsequent usage,

$$\omega_N^{*} = \omega_{N,R} + \mathbf{j}\omega_{N,I} \quad \text{and} \quad b_{NM}^{*} = b_{NM,R} + \mathbf{j} b_{NM,I}.$$

4. REGIONS OF INSTABILITY

The boundaries of the regions of instability for simple and combination resonances are obtained using the following conditions [17].

Case (1): for the simple resonance case, the regions of instability are given by

$$\left| \frac{\bar{\omega}}{2} - \omega_{\mu,R} \right| < \frac{1}{4} \chi_\mu, \quad \mu = 1, 2, \ldots, r, \tag{11}$$

where

$$\chi_\mu = \left[\frac{4\epsilon^2(b_{\mu\mu,R}^2 + b_{\mu\mu,I}^2)}{\omega_{\mu,R}^2} - 16\omega_{\mu,I}^2\right]^{1/2}. \quad (12)$$

Case (2): for combination resonance of the sum type, the regions of instability are given by

$$|\bar{\omega} - (\omega_{\mu,R} + \omega_{\nu,R})| < \chi_{\mu\nu},$$

$$\mu \neq \nu, \quad \mu, \nu = 1, 2, \ldots, r, \quad (13)$$

where

$$\chi_{\mu\nu} = \frac{(\omega_{\mu,I} + \omega_{\nu,I})}{4(\omega_{\mu,I}\omega_{\nu,I})^{1/2}} \times \left[\frac{4\epsilon^2(b_{\mu\nu,R}b_{\nu\mu,R} + b_{\mu\nu,I}b_{\nu\mu,I})}{\omega_{\mu,R}\omega_{\nu,R}} - 16\omega_{\mu,I}\omega_{\nu,I}\right]^{1/2}, \quad (14)$$

when damping is present, and

$$\chi_{\mu\nu} = \epsilon\left[\frac{b_{\mu\nu,R}b_{\nu\mu,R}}{\omega_{\mu,R}\omega_{\nu,R}}\right]^{1/2} \quad (15)$$

in the undamped case.

Case (3): for combination resonance of the difference type, the instability regions are given by

$$|\bar{\omega} - (\omega_{\nu,R} - \omega_{\mu,R})| < \Lambda_{\mu\nu},$$

$$\nu > \mu, \quad \mu, \nu = 1, 2, \ldots, r, \quad (16)$$

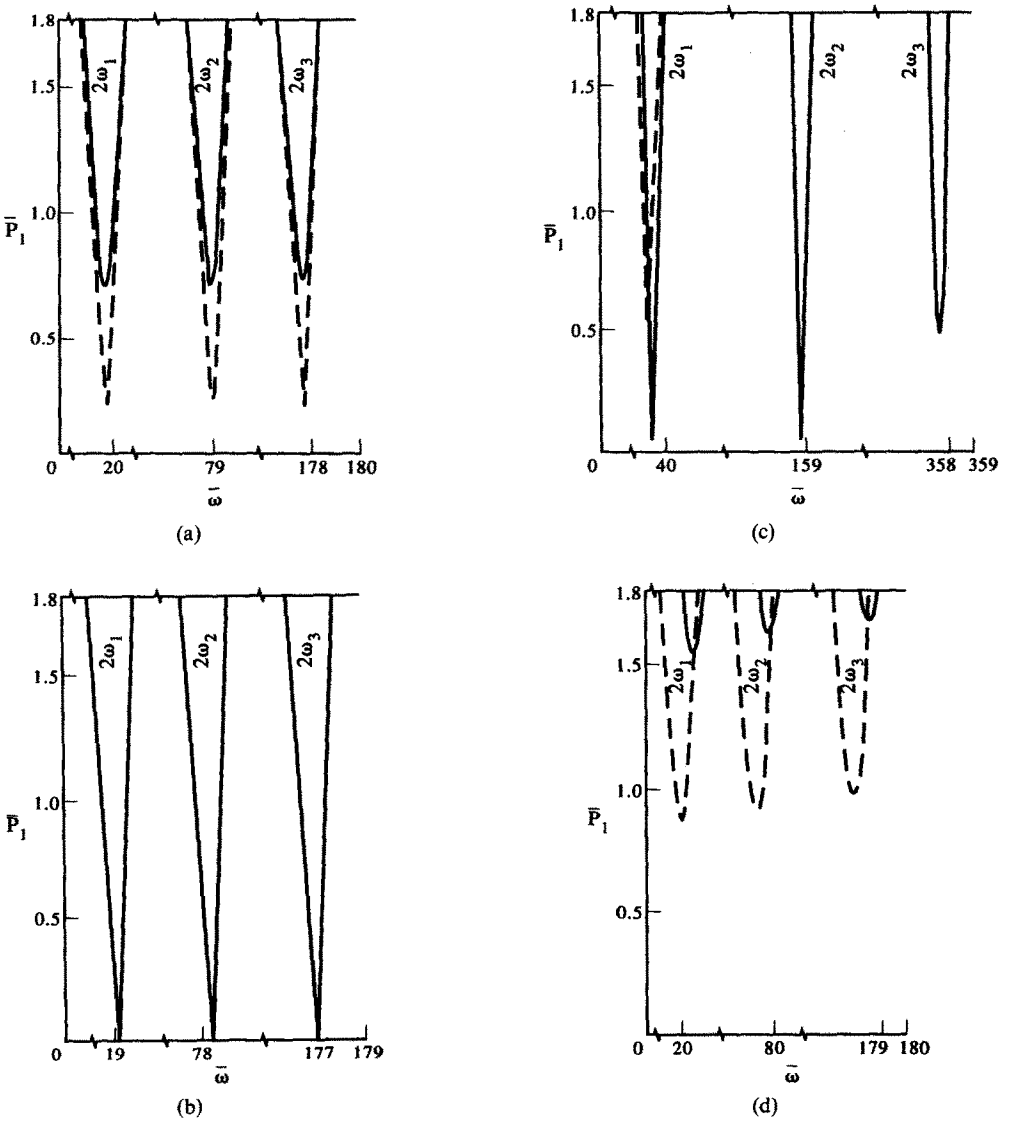

Fig. 5. The P–P case. (a) $h_2/h_1 = 1$, $g = 0.05$; —— $\eta_c = 0.18$; —— $\eta_c = 0.6$. (b) Regions of parametric instability for the reference Euler beam. (c) $h_2/h_1 = 0.01$, $\eta_c = 0.6$; —— $g = 0.05$; —— $g = 5.0$. (d) $\eta_c = 0.6$, $g = 0.05$; —— $h_2/h_1 = 0.5$; —— $h_2/h_1 = 0.8$.

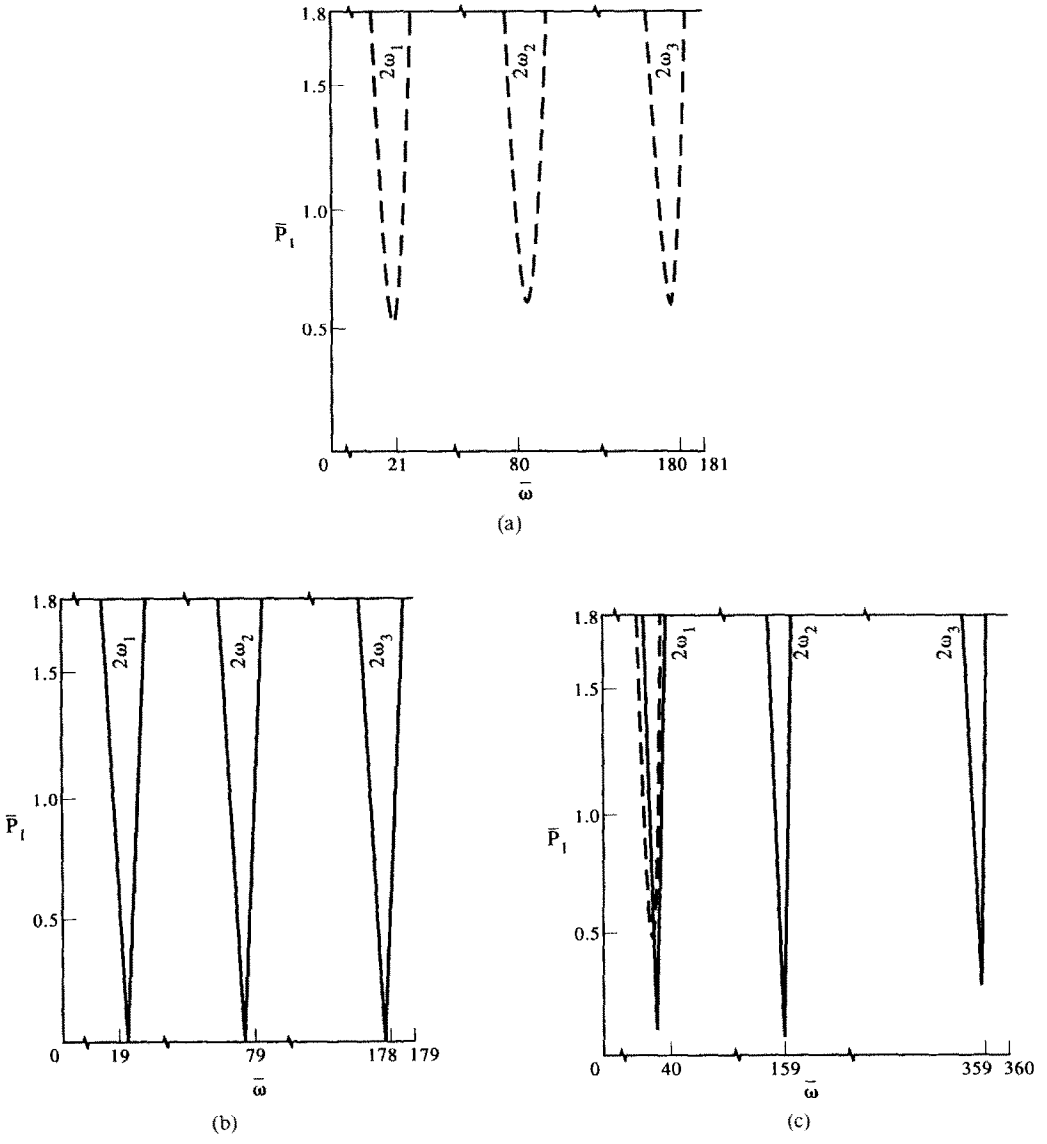

Fig. 6. The P–PR case. (a) $h_2/h_1 = 1$, $g = 0.05$; —— $\eta_c = 0.18$. (b) Regions of parametric instability for the reference Euler beam. (c) $h_2/h_1 = 0.01$, $\eta_c = 0.6$; —— $g = 0.05$; —— $g = 5.0$.

where

$$\Lambda_{\mu\nu} = \frac{(\omega_{\mu,I} + \omega_{\nu,I})}{4(\omega_{\mu,I}\omega_{\nu,I})^{1/2}} \times \left[\frac{4\epsilon^2(b_{\mu\nu,I}b_{\nu\mu,I} - b_{\mu\nu,R}b_{\nu\mu,R})}{\omega_{\mu,R}\omega_{\nu,R}} - 16\omega_{\mu,I}\omega_{\nu,I}\right]^{1/2}, \tag{17}$$

when damping is present, and

$$\Lambda_{\mu\nu} = \epsilon\left[\frac{-b_{\mu\nu,R}b_{\nu\mu,R}}{\omega_{\mu,R}\omega_{\nu,R}}\right]^{1/2} \tag{18}$$

for the undamped case.

5. NUMERICAL RESULTS AND DISCUSSION

The system loss and frequency factors (parameters) were obtained for relevant values of system parameters and these were compared with those given by Rao [9] and good agreement was observed. Also, the first three natural frequencies were obtained for the reference Euler beam corresponding to each boundary condition and the results obtained were found to agree with those reported in [18]. A reference Euler beam corresponding to a given sandwich beam is defined as [9] a homogeneous undamped beam having the same mass per unit length and flexural rigidity as the sandwich beam. Furthermore, the regions of instability for the simple resonance cases, as obtained by the present method, were compared and found to be in good agreement

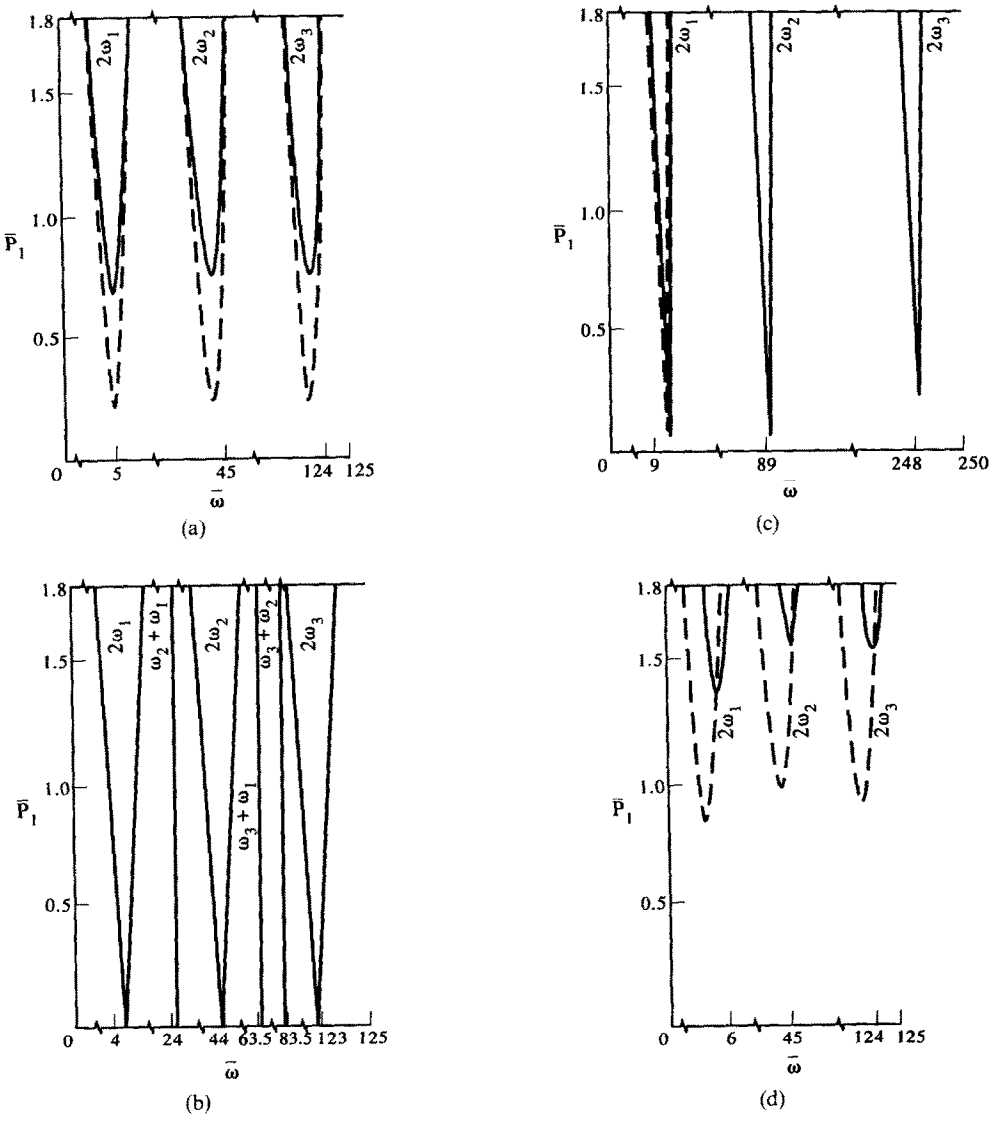

Fig. 7. The G–P case. (a) $h_2/h_1 = 1$, $g = 0.05$; —— $\eta_c = 0.18$; —— $\eta_c = 0.6$. (b) Regions of parametric instability for the reference Euler beam. (c) $h_2/h_1 = 0.01$, $\eta_c = 0.06$; —— $g = 0.05$; —— $g = 5.0$. (d) $\eta_c = 0.6$, $g = 0.05$; —— $h_2/h_1 = 0.5$; —— $h_2/h_1 = 0.8$.

with those obtained by Bolotin's method [19] modified for the complex case. In Figs 2–13(d), $G_2/E_1 = 0.0002$.

Figure 2 shows the effect of shear parameter g on the non-dimensional static buckling load $\bar{P}_{b1}$. It can be seen that $\bar{P}_{b1}$ increases monotonically with g for all the boundary conditions.

The variation of η_1 (the fundamental system loss factor) with the static load parameter $(\bar{P}_0/\bar{P}_{b1})$ is presented in Fig. 3; η_1 is seen to increase monotonically with $(\bar{P}_0/\bar{P}_{b1})$ for all the boundary arrangements considered. Figure 4 shows the influence of the core thickness parameter (h_2/h_1) on η_1. Once again, for all the boundary conditions considered, η_1 increases with (h_2/h_1) for $0.01 \leqslant h_2/h_1 \leqslant 1.0$. For small h_2/h_1, the rate of increase is almost the same for all the cases.

Figures 5(a)–13(d) show the regions of parametric instability corresponding to the first three $\omega_{N,R}$. In these figures, $\omega_{N,R}$ is written as ω_N $(N = 1, 2, 3)$ for brevity.

Figures 5(a), 6(a), . . . , 13(a) show the influence of the core loss factor η_c upon the instability regions and Figs 5(b), 6(b), . . . , 13(b) respectively show the zones of instability for the corresponding undamped reference Euler beams. It can be seen that the introduction, as well as the increase, of core damping improves stability by shifting the zones upwards and reducing their areas for all the boundary cases. In the presence of core damping, however, the zones undergo a minor shift towards higher excitation frequencies. For all the boundary conditions, except the P–P case, a few of the instability zones disappear as η_c is increased to 0.6.

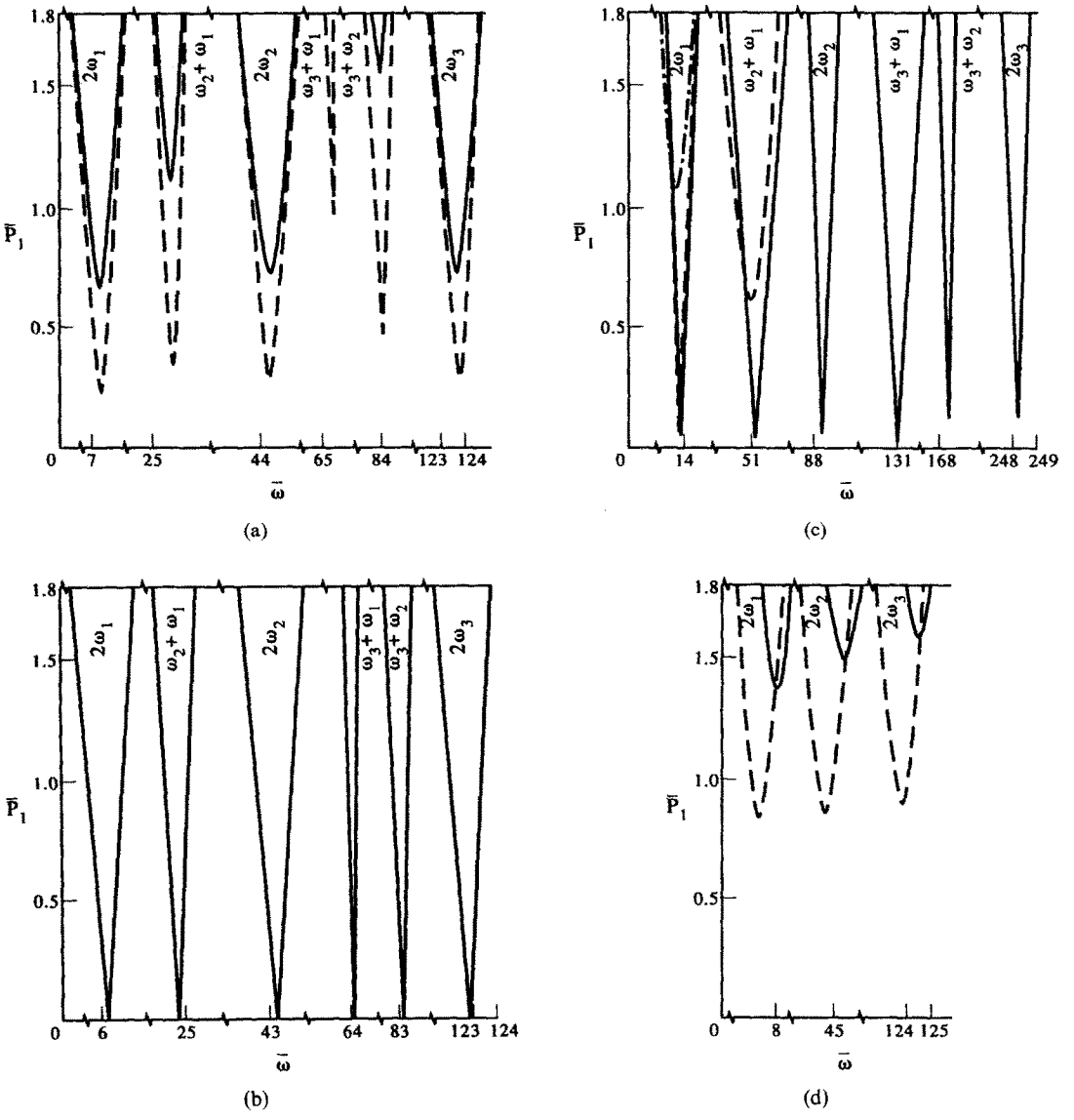

Fig. 8. The C–F case. (a) $h_2/h_1 = 1$, $g = 0.05$; — — $\eta_c = 0.18$; —— $\eta_c = 0.6$. (b) Regions of parametric instability for the reference Euler beam. (c) $\eta_c = 0.6$; —— $g = 5.0$, $h_2/h_1 = 0.01$; — — $g = 0.05$, $h_2/h_1 = 0.01$; — · — $g = 0.05$, $h_2/h_1 = 0.05$. (d) $\eta_c = 0.6$, $g = 0.05$; —— $h_2/h_1 = 0.5$; — — $h_2/h_1 = 0.8$.

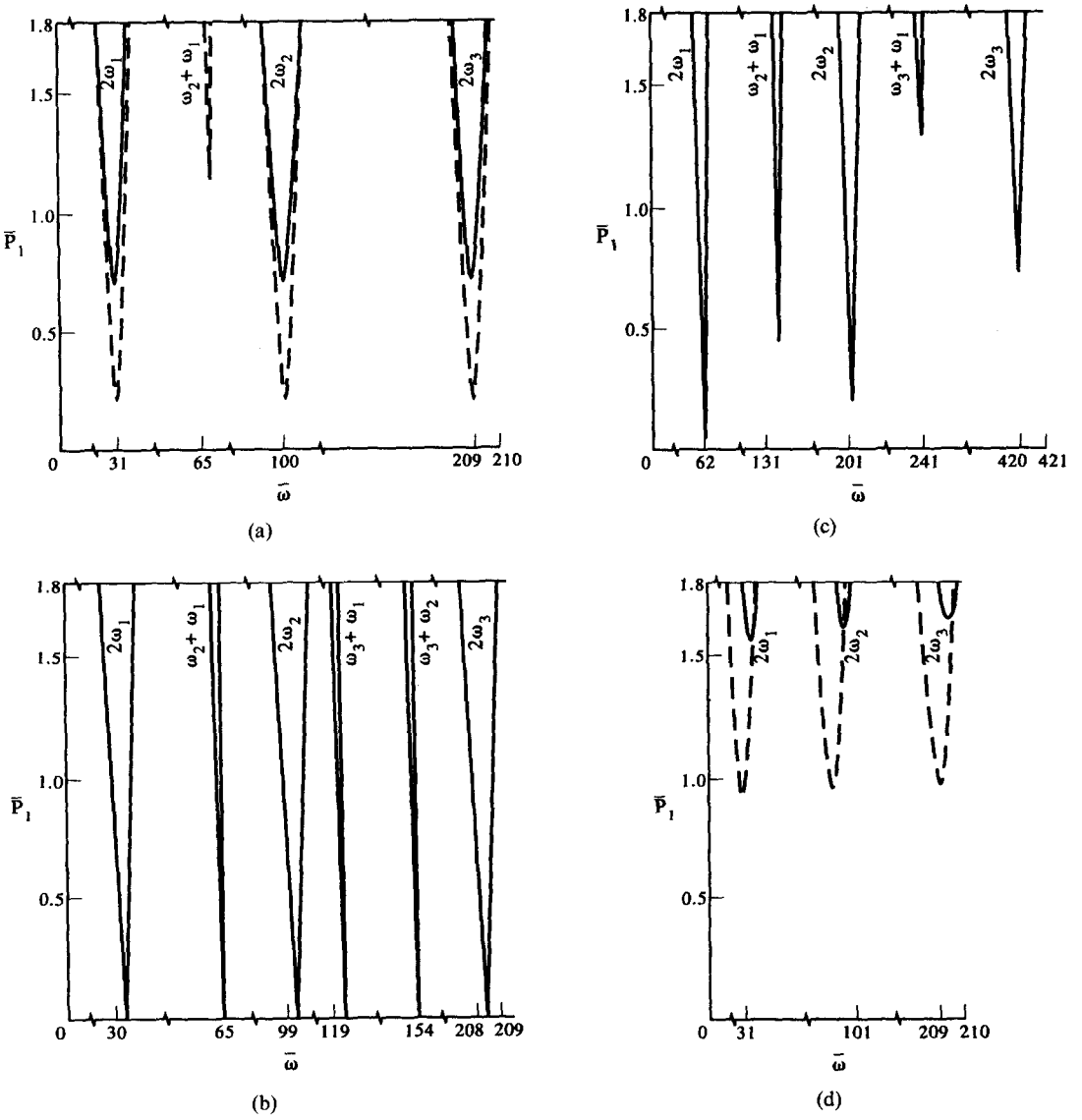

Fig. 9. The C–P case. (a) $h_2/h_1 = 1$, $g = 0.05$; —— $\eta_c = 0.18$; —— $\eta_c = 0.6$. (b) Regions of parametric instability for the reference Euler beam. (c) $h_2/h_1 = 0.01$, $\eta_c = 0.6$, $g = 5.0$. (d) $\eta_c = 0.6$, $g = 0.05$; —— $h_2/h_1 = 0.5$; —— $h_2/h_1 = 0.8$.

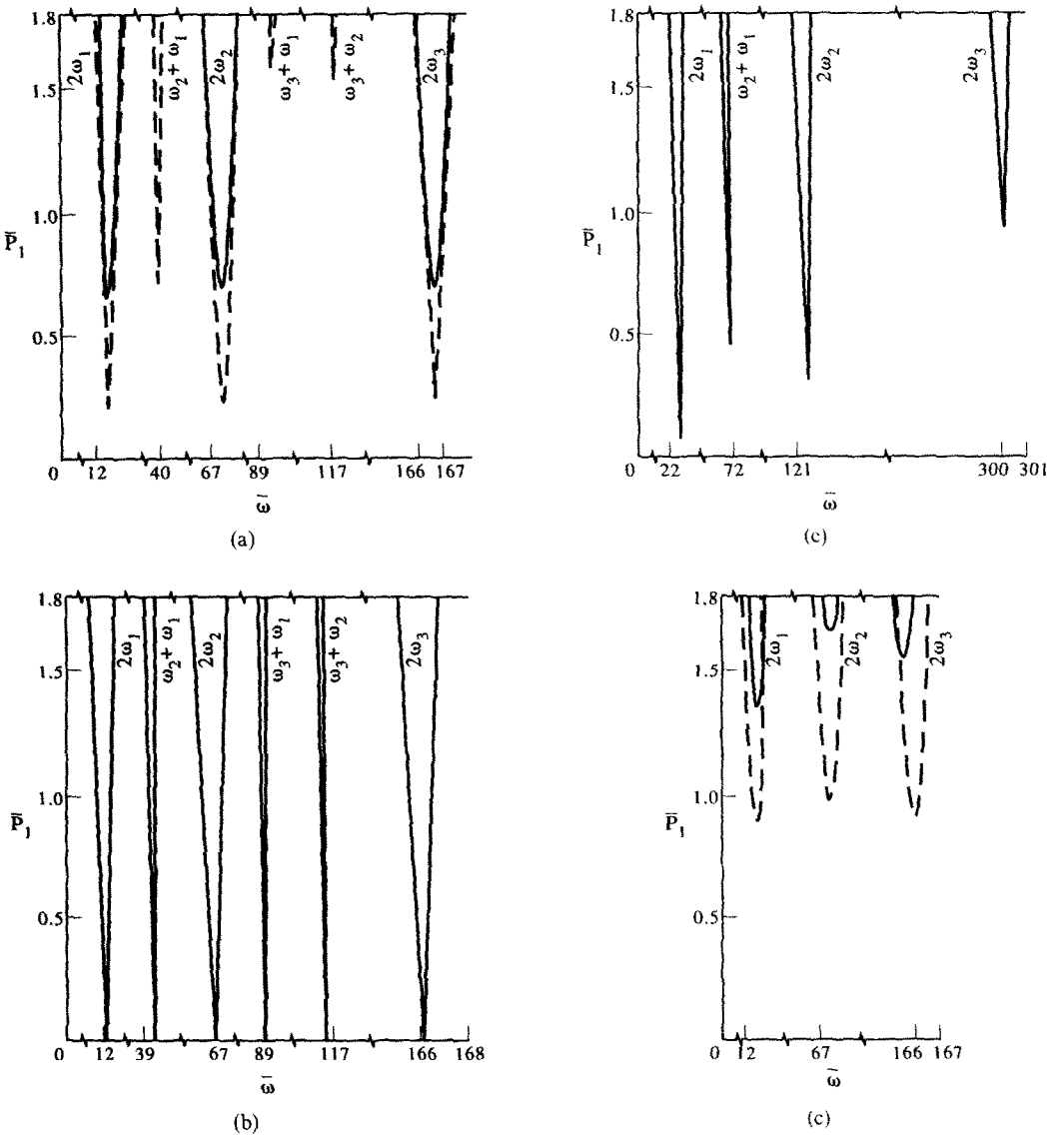

Fig. 10. The C–G case. (a) $h_2/h_1 = 1$, $g = 0.05$; —— $\eta_c \approx 0.18$; —— $\eta_c = 0.6$. (b) Regions of parametric instability for the reference Euler beam. (c) $h_2/h_1 = 0.01$, $\eta_c = 0.6$, $g = 5.0$. (d) $\eta_c = 0.6$, $g = 0.05$; —— $h_2/h_1 = 0.5$; —— $h_2/h_1 = 0.8$.

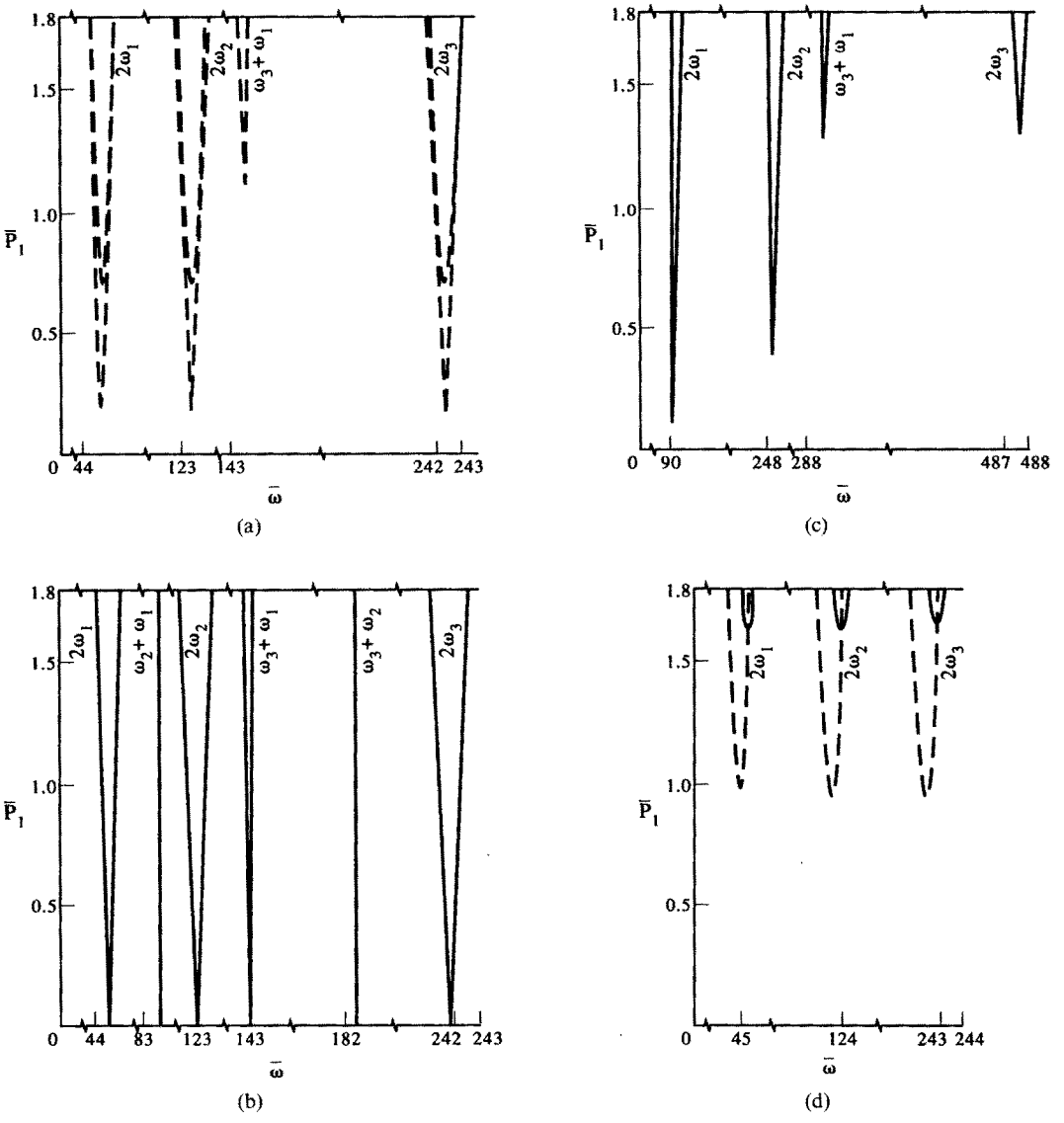

Fig. 11. (a) The C–C case. $h_2/h_1 = 1$, $g = 0.05$; —— $\eta_c = 0.18$; —— $\eta_c = 0.6$. (b) Regions of parametric instability for the reference Euler beam. (c) $h_2/h_1 = 0.01$, $\eta_c = 0.6$, $g = 5.0$. (d) $\eta_c = 0.6$, $g = 0.05$; —— $h_2/h_1 = 0.5$; —— $h_2/h_1 = 0.8$.

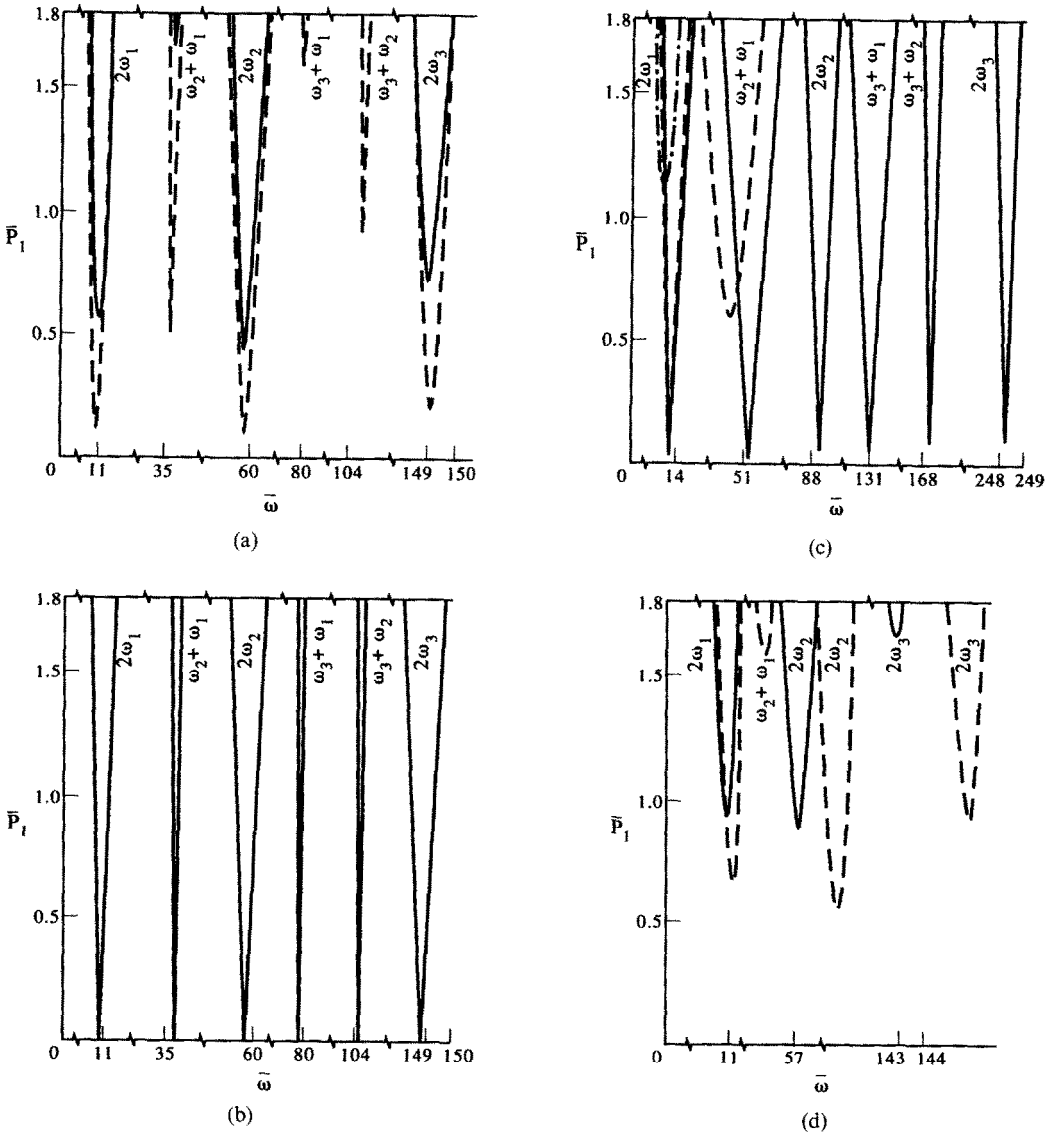

Fig. 12. The C–FR case. (a) $h_2/h_1 = 1$, $g = 0.05$; — — $\eta_c = 0.18$; —— $\eta_c = 0.6$. (b) Regions of parametric instability for the reference Euler beam. (c) $\eta_c = 0.6$; —— $g = 5.0$, $h_2/h_1 = 0.01$; — — $g = 0.05$, $h_2/h_1 = 0.01$; — · — $g = 0.05$, $h_2/h_1 = 0.05$. (d) $\eta_c = 0.6$, $g = 0.05$; —— $h_2/h_1 = 0.5$; — — $h_2/h_1 = 0.8$.

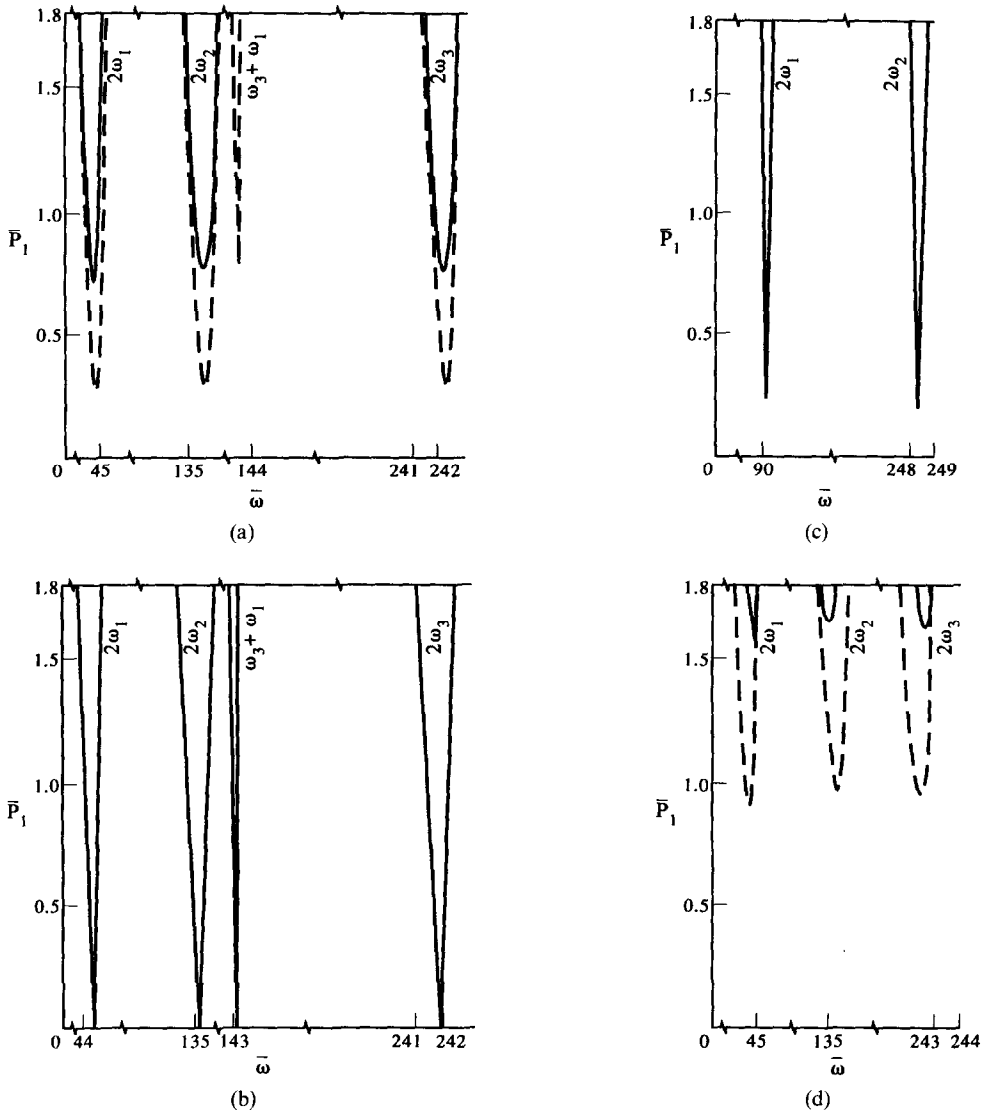

Fig. 13. The C–CUR case. (a) $h_2/h_1 = 1$, $g = 0.05$; —— $\eta_c = 0.18$; —— $\eta_c = 0.6$. (b) Regions of parametric instability for the reference Euler beam. (c) $h_2/h_1 = 0.01$, $\eta_c = 0.6$, $g = 5.0$. (d) $\eta_c = 0.6$, $g = 0.05$; —— $h_2/h_1 = 0.5$; —— $h_2/h_1 = 0.8$.

From Figs 5(c), 6(c), ..., 13(c), it can be seen that an increase in the value of g from 0.05 to 5 has a destabilizing effect, since the area, as well as the number, of the instability zone has increased for all boundary conditions. In the C–P, C–G, C–C and C–CUR cases, all zones disappear for $g = 0.05$.

Fixing upon any of the boundary conditions and considering the corresponding instability diagrams for $g = 0.05$ and $\eta_c = 0.6$ (for instance, Figs 5(c), 5(d), 5(a), etc.), it can be observed that as the h_2/h_1 ratio increases from 0.01 to 1.0, stability may improve or worsen depending upon the value of h_2/h_1. For $h_2/h_1 = 0.05$, $g = 0.05$ and $\eta_c = 0.6$, unstable zones are seen to exist near $2\omega_1$ for the C–F [Fig. 8(c)] and C–FR [Fig. 12(c)] cases only. Thus, for $0.01 \leqslant h_2/h_1 \leqslant 1.0$, the core thickness parameter has a complicated influence upon the zones of instability. However, further study showed that for $h_2/h_1 > 1.0$, stability worsened steadily with an increase in the core thickness parameter for all the boundary conditions.

Finally, comparing Figs 5(a) and 8(a) with Figs 6(a) and 12(a) respectively, it can be noted that riveting can improve stability.

6. CONCLUSIONS

The non-dimensional fundamental static buckling load increases with the shear parameter for all the boundary cases considered. The fundamental system loss factor is also seen to increase with the static load parameter, as well as the core thickness parameter, for all boundary conditions.

Whereas an increase in the core loss factor improves system stability, an increase in the value of the shear parameter has a detrimental effect. The core thickness parameter has a stabilizing or destabilizing effect, depending upon its value. However, riveting is seen to improve stability.

REFERENCES

1. E. M. Kerwin Jr, Damping of flexural waves by a constrained viscoelastic layer. *J. Acoust. Soc. Am.* **31,** 952–962 (1959).
2. R. A. DiTaranto, Theory of vibratory bending for elastic and viscoelastic layered finite-length beams. *J. Appl. Mech. Trans. ASME* **87,** 881–886 (1965).
3. D. J. Mead and S. Markus, The forced vibration of a three-layer, damped sandwich beam with arbitrary boundary conditions. *J. Sound Vibr.* **10,** 163–175 (1969).
4. N. T. Asnani and B. C. Nakra, Vibration analysis of multilayered beams with alternate elastic and viscoelastic layers. *J. Inst. Engineers (Ind.) Mech. Engng Div.* **50,** 187–193 (1970).
5. N. T. Asnani and B. C. Nakra, Vibration damping characteristics of multilayered beams with constrained viscoelastic layers. *J. Engng Indus. Trans. ASME B* **98,** 895–901 (1976).
6. D. K. Rao, Transverse vibrations of pre-twisted sandwich beams. *J. Sound Vibr.* **44,** 159–168 (1976).
7. D. K. Rao, and W. Stühler, Frequency and loss factors of tapered symmetric sandwich beams. *J. Appl. Mech. Trans. ASME* **99,** 511–513 (1977).
8. D. K. Rao, Vibration of short sandwich beams. *J. Sound Vibr.* **52,** 253–263 (1977).
9. D. K. Rao, Frequency and loss factors of sandwich beams under various boundary conditions. *J. Mech. Engng Sci.* **20,** 271–282 (1978).
10. D. K. Rao, Forced vibration of a damped sandwich beam subjected to moving forces. *J. Sound Vibr.* **54,** 215–227 (1977).
11. C. L. Ko, Flexural behaviour of a rotating sandwich tapered beam. *AIAA J.* **27,** 359–369 (1989).
12. N. R. Bauld Jr, Dynamic stability of sandwich columns under pulsating axial loads. *AIAA J.* **5,** 1514–1516 (1967).
13. S. Chonan, Vibration and stability of a two-layered beam with imperfect bonding. *J. Acoust. Soc. Am.* **72,** 208–213 (1982).
14. S. Chonan, Vibration and stability of sandwich beams with elastic bonding. *J. Sound Vibr.* **85,** 525–537 (1982).
15. R. C. Kar and T. Sujata, Dynamic stability of a tapered symmetric sandwich beam. *Comput. Struct.* **40,** 1441–1449 (1991).
16. C. S. Hsu, On the parametric excitation of a dynamic system having multiple degrees of freedom. *J. Appl. Mech. Trans. ASME* **30,** 367–372 (1963).
17. H. Saito and K. Otomi, Parametric response of viscoelastically supported beams. *J. Sound Vibr.* **63,** 169–178 (1979).
18. W. C. Hurty and M. F. Rubinstein, *Dynamics of Structures.* Prentice-Hall, New Delhi (1967).
19. V. V. Bolotin, *The Dynamic Stability of Elastic Systems.* Holden-Day, San Francisco (1964).